

RESEARCH ARTICLE

An Explainable Artificial Intelligence Integrated System for Automatic Detection of Dengue From Images of Blood Smears Using Transfer Learning

HILDA MAYROSE¹, NIRANJANA SAMPATHILA¹, (Senior Member, IEEE),
G. MURALIDHAR BAIRY¹, (Senior Member, IEEE), TUSHAR NAYAK¹, (Member, IEEE),
SUSHMA BELURKAR², AND KAVITHA SARAVU³

¹Department of Biomedical Engineering, Manipal Institute of Technology, Manipal Academy of Higher Education (MAHE), Manipal 576104, India

²Department of Pathology, Kasturba Medical College, Manipal Academy of Higher Education (MAHE), Manipal 576104, India

³Department of Infectious Diseases, Kasturba Medical College, Manipal Academy of Higher Education (MAHE), Manipal 576104, India

Corresponding authors: G. Muralidhar Bairy (gm.bairy@manipal.edu) and Niranjana Sampathila (niranjana.s@manipal.edu)

ABSTRACT Dengue fever is a rapidly increasing mosquito-borne ailment spread by the virus DENV in the tropics and subtropics worldwide. It is a significant public health problem and accounts for many deaths globally. Implementing more effective methods that can more accurately detect dengue cases is challenging. The theme of this digital pathology-associated research is automatic dengue detection from peripheral blood smears (PBS) employing deep learning (DL) techniques. In recent years, DL has been significantly employed for automated computer-assisted diagnosis of various diseases from medical images. This paper explores pre-trained convolution neural networks (CNNs) for automatic dengue fever detection. Transfer learning (TL) is executed on three state-of-the-art CNNs – ResNet50, MobileNetV3Small, and MobileNetV3Large, to customize the models for differentiating the dengue-infected blood smears from the healthy ones. The dataset used to design and test the models contains 100x magnified dengue-infected and healthy control digital microscopic PBS images. The models are validated with a 5-fold cross-validation framework and tested on unseen data. An explainable artificial intelligence (XAI) approach, Gradient-weighted Class Activation Mapping (GradCAM), is eventually applied to the models to allow visualization of the precise regions on the smears most instrumental in making the predictions. While all three transferred pre-trained CNN models performed well (above 98% overall classification accuracy), MobileNetV3Small is the recommended model for this classification problem due to its significantly less computationally demanding characteristics. Transferred pre-trained CNN based on MobileNetV3Small yielded Accuracy, Recall, Specificity, Precision, F1 Score, and Area Under the ROC Curve (AUC) of 0.982 ± 0.011 , 0.973 ± 0.027 , 0.99 ± 0.013 , 0.989 ± 0.015 , 0.981 ± 0.012 and 0.982 ± 0.012 respectively, averaged over the five folds on the unseen dataset. Promising results show that the developed models have the potential to provide high-quality support to haematologists by expertly performing tedious, repetitive, and time-consuming tasks in hospitals and remote/low-resource settings.

INDEX TERMS Deep learning, dengue fever, digital pathology, explainable artificial intelligence, GradCAM, peripheral blood smear, pre-trained CNN, transfer learning.

The associate editor coordinating the review of this manuscript and approving it for publication was Ines Domingues¹.

I. INTRODUCTION

Dengue, an *Aedes aegypti* and *Aedes albopictus* mosquito-borne illness, emerged as a global health problem in the 1960s

[1]. One study on the prevalence of dengue indicates that about half of the global population is in danger, with an annual estimate of 100-400 million infections [1]. Another study estimates that about 3-9 billion people are vulnerable to the dengue virus in >100 countries where the disease is endemic [2]. As per a recent report on dengue by WHO, the Americas, Southeast Asia, and Western Pacific regions are dangerously affected, with Asia experiencing 70% of the overall burden [3]. India is among the 30 most highly endemic countries in the world [3]. Despite decades of attempts, a safe and efficacious vaccine or anti-viral drug for dengue is not in place [4]. Although many DENV infections cause mild illness, severe dengue has been the primary cause of morbidity and mortality in the dengue endemic regions. Severe dengue is characterized by severe plasma leakage, fluid accumulation with respiratory distress or shock, severe organ impairment, and severe bleeding [5]. To date, there is no precise treatment in place for dengue, and the death rates can only be reduced by early detection of severe dengue [3]. Several methods are currently available to detect DENV infection, including isolation of the virus, serology methods, or RT-PCR [5], [6]. Medical laboratories in remote/low-resource settings lack specialized resources for the diagnosis of dengue by any means other than serology methods [5]. Among serological techniques, the detection of non-structural protein 1 (NS1) antigen and Immunoglobulin M (IgM)/Immunoglobulin G (IgG) antibodies are commonly used. NS1 antigen-capture ELISA is a simple efficacious diagnostic tool that supplies qualitative positive/negative results [5], [7]. IgM and IgG antibody-capture ELISAs are beneficial in finding out whether the DENV infection is recent or previous [5], [6].

This paper focuses on an alternative method of identifying dengue infection through a digital pathology approach from microscopic PBS images. The PBS analysis is a diagnostically relevant tool for evaluating various hematological disorders [8]. The manual interpretation of PBS through a microscope remains the backbone of hematological diagnostics, even though it is error-prone and time-consuming owing to its invaluable nature [9]. Automation of PBS analysis is a very active field of research that has motivated many researchers [8]. Automation can assist hematologists in yielding accurate and quick results, especially when there are tremendous amounts of samples to analyze. The digitization of PBS images using a digital microscope or a whole slide scanner, combined with the application of Artificial Intelligence (AI) – based tools, makes automated PBS image analysis feasible, limiting human intervention [8], [9].

In recent years, DL, a subset of AI, has been extensively and successfully used for automating various tasks, including healthcare-related tasks [10]. In particular, CNNs have gained popularity and become the main methodology for medical image analysis [10]. Digital pathology is one of the medical imaging areas where extensive use of CNNs is observed [10]. Whole-slide imaging systems are applied to digitize hematopathology/histopathology slides to generate images of high resolution [10]. The digitized slides are

processed by incorporating CNN architectures to perform different computer vision tasks, which include classification (e.g., disease recognition), object detection (e.g., cell counting), and segmentation (e.g., nuclei identification) [10]. The ability of CNNs to extract high-level features without human supervision enables them to automatically learn the most discriminative features directly from the image [9], [11]. In particular, CNNs benefit from eliminating the tedious feature engineering process [12]. However, training from scratch demands a significantly huge labeled dataset. The inadequacy of freely accessible labeled images is one of the biggest hindrances in training CNNs for analysis of medical images (including digital pathology images) [10], [12]. An efficient solution in such a scenario is to employ pre-trained CNNs [12].

A pre-trained CNN is previously trained on millions of images from a generic dataset (e.g., ImageNet dataset) for a specific problem and could be employed to fix a fresh problem using a TL plan [10], [12]. TL signifies fine-tuning the model to fix a fresh problem [12]. The Fully Connected (FC) layers with randomly initialized weights are added to the pre-trained base model and trained on the new task-specific dataset during fine-tuning [13]. However, the base model weights are frozen to prevent them from getting updated during training to avert overfitting [13]. Commonly used CNN architectures for the analysis of medical images include AlexNet, VGGNet, ResNet, GoogLeNet, DenseNet, XceptionNet, and SqueezeNet [12]. These CNNs are trained to identify images into 1000 subcategories [14]. The advantages of transferred pre-trained CNNs include better performance, training with limited data, eliminating training from scratch, and speeding up the training process [12].

Lack of explainability is one main limitation of DL models [15], [16]. The logic behind the predictions made by these models is not clearly understood. Despite the excellent performance of the DL models in various healthcare applications, the medical fraternity still does not fully embrace them due to their black-box nature [17], [18]. The XAI technique was introduced to enable the medical fraternity to appreciate the philosophy behind the model predictions [17]. XAI explains the workings of the model and draws the users' attention to the regions of the image that highly influence the model predictions [17]. The GradCAM XAI technique was built on the original CAM invented by Zhou et al. in 2015 [17], [19], [20]. GradCAM was developed to suit CNN architectures and is, therefore, more popular among DL models [15], [17].

A. REVIEW OF RELATED LITERATURE

In recent years, enormous CNN architectures with TL have been put forward to analyze medical images, including digital pathology image analysis [10]. The following are some recently published articles that adopted pre-trained CNN architectures with a TL strategy for classifying leukocytes from digital microscopic PBS images.

Aziz et al. adopted a DL-based method for leukocyte classification (Munich AML Morphology dataset) from blood

smear images. Leukocytes were segmented using K-means clustering in the color space - L^*a^*b . The authors performed classification by employing transferred pre-trained AlexNet and ResNet18. Classification accuracies of 93.30% for AlexNet, and 93.85% for ResNet18 were achieved [21]. Roy et al. presented a method for localizing and classifying leukocytes (LISC dataset) using a DL approach. The authors localized the leukocytes by semantic segmentation using DeepLabv3+ and cropped the leukocytes. Further, the cropped leukocytes were classified by employing pre-trained AlexNet with TL. An average classification accuracy of 98.87% [22] was observed. Khaled et al. explored transferred pre-trained CNNs - VGG, ResNet, and DenseNet for classifying different leukocytes (LISC dataset). The cropped leukocytes were augmented by using image transformations and generative adversarial networks (GAN). A classification accuracy of 98.8% using DenseNet-169 [23] was obtained. Li et al. combined GAN with ResNet to classify leukocytes (BCCD dataset). The authors adopted GAN for increasing the training data, transferred pre-trained ResNet for the classification, and reported an accuracy of 91.7% with a modified loss function [24]. Sharma et al. presented a strategy for the automatic leukocyte classification (Kaggle dataset) using pre-trained CNN DenseNet121. With augmentation and transfer learning, a classification accuracy of 98.84% was achieved [25]. Cengil et al. employed pre-trained CNN architectures - AlexNet, ResNet18, and GoogleNet, with TL for automatically classifying leukocytes (Kaggle dataset). ResNet18 yielded the best classification accuracy of 99.83% [26]. Liu et al. put forward a DL technique for the leukocyte classification. Various pre-trained CNNs were employed. ResNet-50 excelled with an average classification accuracy of 96.7% over C-NMC, ALL-IDB2, PBC, and LISC datasets [27]. Chen et al. proposed a DL framework by integrating two pre-trained networks - ResNet and DenseNet with an attention system for accurately classifying the cropped leukocytes. An overall classification accuracy of 97.96% and 98.71% for the LISC and Raabin datasets, respectively, was achieved with data augmentation and transfer learning. The GradCAM XAI technique was employed to understand the logic behind the predictions made by the model [28]. Meenakshi et al. adopted deep features extracted from CNNs that are pre-trained for automatically classifying leukocytes. The authors extracted 3,000 deep features, 1,000 each from pre-trained CNNs AlexNet, GoogleNet, and ResNet50. Mayfly Algorithm with Particle Swarm Optimization was used to select the most important 1,000 features. These features were then given to the RNN - LSTM classifier to perform the classification. An overall classification accuracy of 95.25% was achieved [29]. Dong et al. developed a novel ensemble CNN framework to classify the five types of leukocytes. The prediction results of the three transferred pre-trained CNN models VGG16, ResNet50, and InceptionV3 were integrated through the Bagging process. The Gompertz function was incorporated to formulate the

combination strategy, which yielded an average classification accuracy of 96.5% with ten-fold cross-validation [30]. Dipto et al. presented a strategy for identifying the types of leukocytes (BCCD dataset) by utilizing a pre-trained vision transformer (VT) and pre-trained CNN VGG19. An overall classification accuracy of 84% and 85% was achieved for VT and VGG19, respectively. However, VT demonstrated significantly faster learning compared to VGG19. The GradCAM XAI technique was integrated to understand the logic behind the predictions made by the model [31]. To classify leukocytes from blood smear images, Bhatia et al. employed various pre-trained DL models, such as DenseNet121, Xception, MobileNetV2, ResNet50, and VGG16. DenseNet121 outperformed with an average classification accuracy of 98.59%. An XAI technique was integrated, thereby leveraging local interpretable model-agnostic explanations (LIME) into the models to make the model's predictions explainable [32].

The unique and distinctive contribution introduced by this proposed work is an XAI-integrated, computationally efficient deep-learning approach for automatically detecting dengue fever from digital microscopic PBS images. PBS analysis is a gold standard for diagnosing various hematological disorders, including dengue fever. The literature review revealed very few published works utilizing similar methodologies on comparable datasets. Most of the published work associated with automatic dengue detection was centered on tabular datasets containing symptoms/vital signs/blood profile data [33], [34], [35], [36]. Hence, this proposed work can potentially fill this gap in the literature. Only a few articles have been published on the automatic diagnosis of dengue from PBS images [37], [38]. In one of our published works [37], we employed MobileNetV2 (a pre-trained CNN) for extracting features of the lymphocyte nucleus. Further, these deep features were administered to popular supervised classifiers to detect dengue-infected smears against the normal ones. A classification accuracy of 95.74% was obtained with the Support Vector Machine (SVM). This paper presents an explainable DL approach for dengue detection from 100x digital microscopic PBS images using pre-trained CNNs with TL. Here, an end-to-end system performs the classification process, bypassing segmentation and feature extraction/selection. To the best of our knowledge, there has been no prior publication on the use of this technique for dengue detection from PBS images.

Significant contributions of this article are listed as follows:

1. Novel end-to-end computationally efficient DL system for automatically detecting dengue from PBS images.
2. Integration of GradCAM XAI technique that provides confidence to the clinicians in the DL model's predictions.
3. Utilizes an original hospital dataset (i.e., microscopic PBS images of dengue-infected and normal controls) collected systematically under ethical clearance.

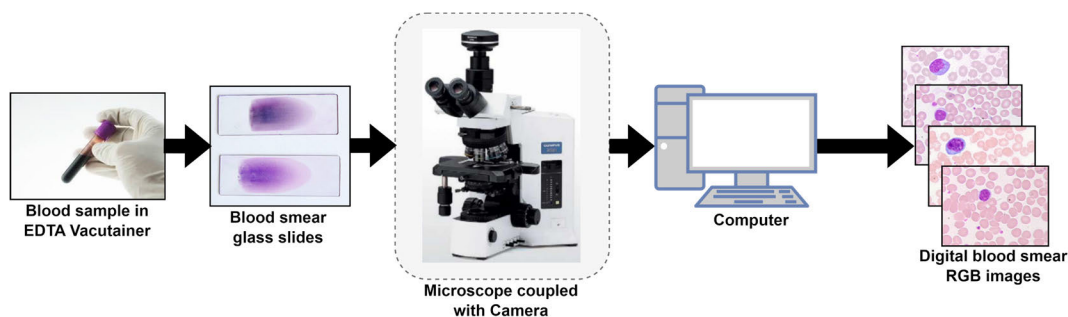


FIGURE 1. Dataset preparation.

The arrangement of the article is as follows. In Section II, the details of the image dataset and the implementation process of the models are presented. Section III provides the detailed experimental results and discussion. Finally, Section IV provides the conclusions and directions for future works.

II. METHODOLOGY

This paper proposes an explainable DL approach for detecting dengue fever from microscopic images of blood smears. State-of-the-art pre-trained CNNs are used to lower the expenses of model training from scratch. Heat maps are generated using the GradCAM XAI technique to highlight which areas on the image are concentrated in the predictions of the CNN model. The clear-cut details concerning the data, and the implementation of the TL and the XAI are described here.

A. IMAGE DATASET

The dataset adopted is authentic hospital data accumulated from the Hematology Lab, Kasturba Hospital, Manipal. The data is acquired under ethical clearance (114/2020) granted by the Institutional Committee. Normal blood samples are collected from the Department of Immunohematology, Kasturba Hospital, Manipal, from blood bank donors visiting the department. Figure 1 shows the dataset preparation process. The dataset contains 888 PBS images (446 dengue-infected and 442 normal controls) garnered from 116 Leishman-stained blood smear thin glass slides (60 dengue-infected and 56 normal controls). A high-quality technology brightfield microscopic imaging system - Olympus DP25 digital microscope facilitated with a 5-megapixel high-precision digital camera and DP2-BSW software is used to capture the digital images of exceptional quality (2560×1920 pixels) from the slides. The microscope is coupled with a camera and linked to a computer. The images captured are in RGB color space with a color depth of eight bits per color channel. First, the body region of the slide is identified by focusing the slide with a 40x objective lens. Then, the images/oil immersion fields (ROIs) are focused and captured with a 100x objective lens with a resolution of $2560 \times 1920 \times 3$. The images are resized to $640 \times 480 \times 3$ due to memory constraints. The dataset is

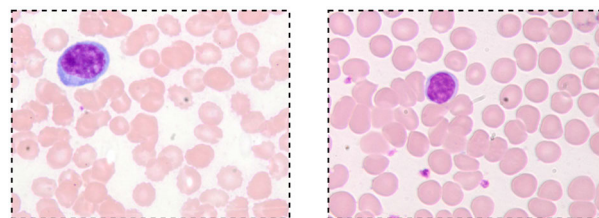


FIGURE 2. PBS images. (a) Dengue-infected and, (b) Normal control.

split up randomly into training and validation, respectively, in a ratio of 4:1.

The emphasis is on the lymphocytes (one among the five types of leukocytes) throughout the work. Dengue alters the morphology of the lymphocytes. Studies show that this is an important indicator for dengue diagnosis [39]. PBS images of dengue-infected and normal control subjects are shown in Figure 2.

B. IMPLEMENTATION DETAILS

TL is executed on three state-of-the-art CNNs – ResNet50, MobileNetV3Small, and MobileNetV3Large and is utilized to discriminate dengue-infected smears from normal. The pipeline for dengue detection from PBS using transferred pre-trained CNNs is displayed in Figure 3.

1) PRE-TRAINED CNNs—RESNET50, MOBILENETV3SMALL, AND MOBILENETV3LARGE

ResNet50 is the most common type of residual network that was introduced in 2015 to address the problems of vanishing gradient and performance degradation associated with deep CNNs [40], [41]. It has 107 layers (49 convolution layers + an FC layer) and approximately 26 million parameters [42]. ResNet50 architecture begins with a convolution layer and is followed by 16 stacked building blocks (residual) and terminates with an FC layer [43], [44]. Each residual block is a bottleneck block consisting of a stack of three convolution layers (1×1 , 3×3 , and 1×1) [41]. The building blocks of ResNet50 utilize residual connections, or skip connections, to propagate information directly through the

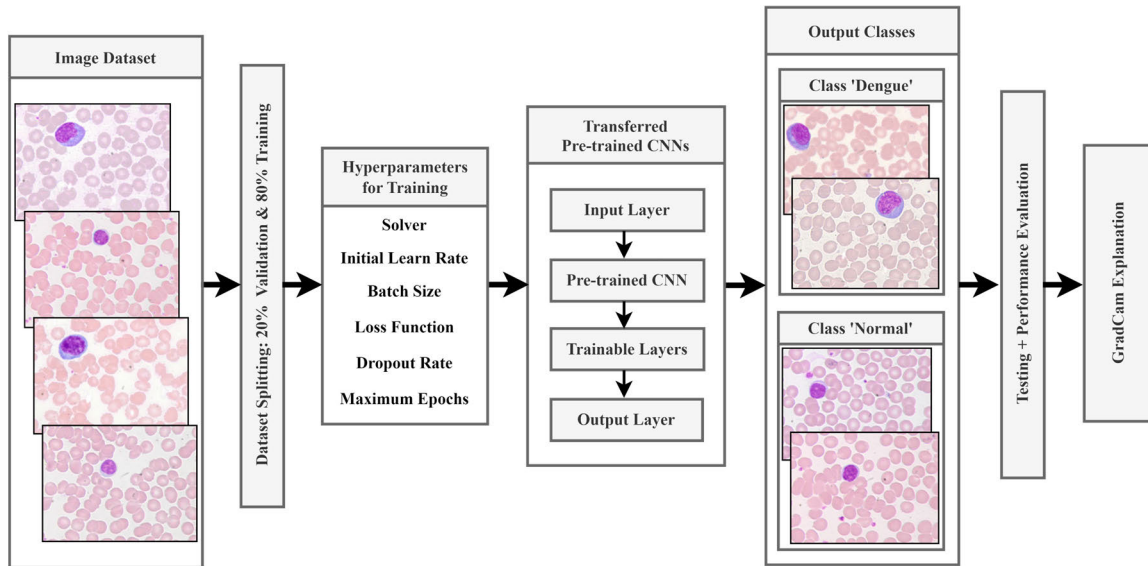


FIGURE 3. Pipeline for the detection of dengue using pre-trained CNNs.

network and overcome the degradation and vanishing gradient problems [41].

MobileNetV3, introduced in 2019, is the latest version of lightweight MobileNets [45], [46]. MobileNetV3 was built upon the MobileNetV1 and V2 structures. MobileNetV1 uses lightweight depth-wise convolutions to reduce the number of parameters [47]. MobileNetV2 was built upon MobileNetV1 with a new resource-efficient feature added: Inverted residual blocks with linear bottlenecking structure [47]. To make the structure more accurate and efficient, MobileNetV3 was introduced. Major improvements in MobileNetV3 include the Squeeze and Excitation - attention module added to the residual block and the use of hard-swish non-linearity instead of ReLU [47]. Moreover, platform-aware network architecture search and NetAdapt algorithm are engaged to optimize the architecture at the block and layer levels, respectively [47], [48]. Furthermore, MobileNetV3 includes small and large versions that operate on the same principle but vary in depth and trainable parameters [45], [49]. These networks have drastically lower parameter counts (approximately 2.9 million for small and approximately 5.4 million for large) and can be effectively implemented on resource-constrained devices [50].

2) TRANSFER LEARNING

The transfer learning plan accommodates the pre-trained CNNs to the dengue dataset. The pre-trained CNNs ResNet50, MobileNetV3Small, and MobileNetV3Large are base models. TL signifies fine-tuning the CNNs to resolve a new problem [12]. During fine-tuning, the trainable layers with randomly initialized weights are added on top of the pre-trained base model and trained on the new task-specific dataset [13]. Trainable layers include a flattened layer, a dense layer with 512 neurons and ReLU activation, a batch

normalization layer, a dropout layer with rate=20%, a dense layer with 256 neurons and ReLU activation, a dropout layer with rate=20%. The output is fed to the final dense layer with two classes and Softmax activation to classify. These layers are added after the frozen base model, as illustrated in Figure 4.

3) HYPERPARAMETERS

The hyperparameters used to train the transferred pre-trained CNN architectures are tabulated in Table 1. These hyperparameters are fine-tuned to attain the optimum performance. Dropout is used after each dense layer to mitigate overfitting by randomly dropping out 20% of the neurons during training. The Learn Rate is initialized to 0.0001, and a scheduler is employed to dynamically decay the Learn Rate by a factor of 0.1 when the validation loss does not improve over four consecutive epochs. The size of the batch is fixed to 32 due to memory constraints, and the network is trained with maximum epochs set to 40. The early stopping mode is triggered to halt the training when the validation loss does not improve over six consecutive epochs, and the best weights are restored.

The randomly initialized weights of the trainable layers are upgraded during the training of the models, depending on the optimization algorithm, to lessen the loss function [51]. Here, the loss function is cross-entropy. Cross-entropy loss is represented by Eq. (1)

$$L_{CE} = - \sum_{i=1}^n t_i \log(p_i) \quad (1)$$

In Eq. (1), n is the number of classes, t_i corresponds to the truth label, and p_i corresponds to the Softmax probability of i^{th} class. Gradient descent is a common optimization algorithm that updates the weights of the network iteratively. The gradient is mathematically represented as a partial derivative of the loss concerning the weight. A single update

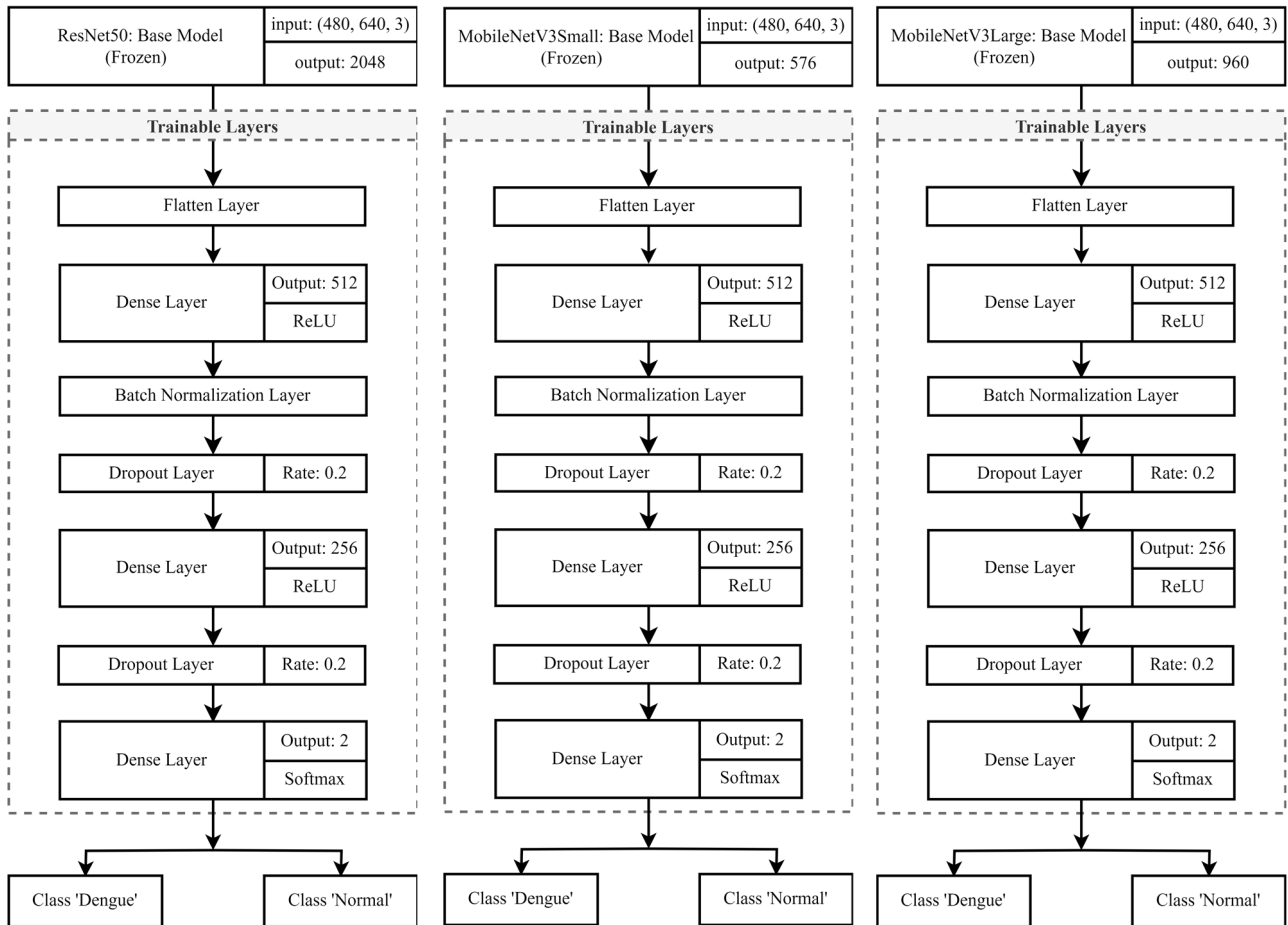


FIGURE 4. The architecture of transferred pre-trained CNNs based on (a) ResNet50 (b) MobileNetV3Small (c) MobileNetV3Large.

of the weight is represented in Eq. (2).

$$w := w - \alpha \partial L / \partial w \tag{2}$$

In Eq. (2), w stands for the weight, α stands for learn rate, and L stands for the loss function. Many improvements to the gradient descent algorithm have been proposed, such as stochastic gradient descent with momentum (sgdm), RMSprop, and Adam [51], [52]. Here, the binary cross-entropy loss during training has been curtailed using an Adam optimizer (Solver). Figure 5 illustrates the pseudo-code for implementing TL for the proposed method.

All the CNN models are executed using Keras (with TensorFlow backend) on Kaggle Notebooks with Nvidia GPU P100 Accelerator (15.9GB RAM) conducted on a 64-bit Laptop with an Intel Core i5-7200U CPU (8GB RAM).

4) GRADCAM EXPLANATIONS

GradCAM is the most extensively employed XAI technique for medical image analysis [17], [53]. It is very often coupled with DL models such as CNNs, which are popular for image recognition [15], [17]. The last convolution layer of a CNN model contains the most discriminative features with detailed spatial information [15], [17]. GradCAM uses the gradients

```

Import libraries: tensorflow, Keras, sklearn
Import dataset: 888 PBS images
Data preprocessing: Resizing (640x480)
Model development: pre-trained base model + Trainable layers
                        added
Dataset splitting: for 5-fold cross-validation (Training 80%,
                        Validation 20%)
Repeat
  Model training for each iteration: with the best combination of
  hyperparameters after tuning
  Model evaluation for each iteration
Until five iterations are complete
  Model evaluation (Average): visualizing loss & accuracy for
  training and validation epoch by epoch,
  confusion matrix, performance metrics for
  validation data, GradCAM visualization
Model testing with unseen data: confusion matrix, performance
  metrics for test (unseen) data
    
```

FIGURE 5. The pseudo-code for the implementation of transfer learning for the proposed work.

of the class score with respect to the feature maps at the final convolution layer to generate heat maps [15], [17]. These heatmaps are then superimposed on the images, which help the users to see the areas of the image that are most valuable

TABLE 1. Hyperparameters used to train the transferred pre-trained CNN architectures

Hyperparameter		Value
Maximum Epochs		40
Batch Size		32
Solver		Adam
Loss Function		Binary Cross Entropy
Learn Rate Decay	Initial Learn Rate	0.0001
	Patience	4 Epochs
	Monitor	Validation Loss
	Factor	0.1
Early Stopping	Patience	6 Epochs
	Monitor	Validation Loss
	Weights	Restore Best Weights
Regularization	Dropout Rate	0.2

for the model predictions. GradCAM follows three steps [15], [18], [54] to generate the heat maps, as shown below:

Step 1: Calculate the class score gradient c, y^c (before the Softmax), with respect to k feature maps A^k of the last convolution layer,

$$\text{i.e. } \frac{\partial y^c}{\partial A^k_{i,j}}$$

Step 2: Global average pool the gradients to obtain the weights α_k^c as given by Eq. (3). This weight picks up the value of feature map k for a target class c .

$$\alpha_k^c = \frac{1}{N} \sum_i \sum_j \frac{\partial y^c}{\partial A^k_{i,j}} \quad (3)$$

In Eq. (3), N represents the pixels in the feature map.

Step 3: The GradCAM map is then a weighted combination of the feature maps with an applied ReLU as given by Eq. (4).

$$M = \text{RELU} \left(\sum_k \alpha_k^c A^k \right) \quad (4)$$

The ReLU activation preserves only the features that have a positive contribution to the class of interest.

III. RESULTS AND DISCUSSION

All three models are assessed using the five-fold cross-validation scheme, wherein the data is split randomly into training (80%) and validation (20%). Further, the models are tested with unseen data. The test dataset contains 78 PBS images, of which 37 are dengue-infected, and 41 are normal controls. Six popular indices – Accuracy, Recall, Specificity, Precision, F1-score, and Area Under the ROC Curve (AUC) are used to gauge the model’s performance. These statistical metrics are derived from true positives (‘Dengue’ correctly

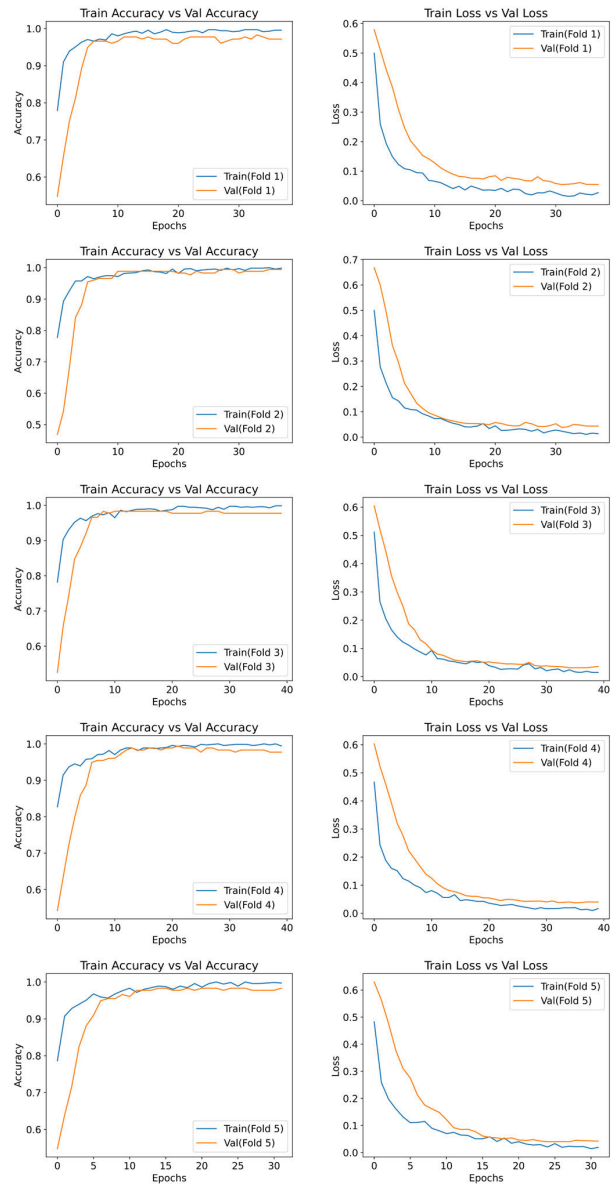


FIGURE 6. Accuracy and Loss plots - Training (Blue) / Validation (Orange) for five folds of the transferred pre-trained CNN based on MobileNetV3Small.

classified; TP), true negatives (‘Normal’ correctly classified; TN), false negatives (‘Dengue’ incorrectly classified as ‘Normal’; FN), and false positives (‘Normal’ incorrectly classified as ‘Dengue’; FP) and are defined in Eq. (5) - (9).

$$\text{Accuracy} = \frac{\text{TP} + \text{TN}}{\text{TP} + \text{TN} + \text{FP} + \text{FN}} \times 100 \quad (5)$$

$$\text{Recall} = \frac{\text{TP}}{\text{TP} + \text{FN}} \times 100 \quad (6)$$

$$\text{Specificity} = \frac{\text{TN}}{\text{FP} + \text{TN}} \times 100 \quad (7)$$

$$\text{Precision} = \frac{\text{TP}}{\text{FP} + \text{TP}} \times 100 \quad (8)$$

$$\text{F1 Score} = \frac{2 * \text{Pre} * \text{Sen}}{\text{Pre} + \text{Sen}} \times 100 \quad (9)$$

TABLE 2. Classification accuracies on the validation dataset for each of the 5 folds and the overall (MEAN ± SD) classification accuracy.

Transferred Pre-trained Models	Accuracy					
	Fold 1	Fold 2	Fold 3	Fold 4	Fold 5	Overall
ResNet50	1.000	0.983	0.989	0.983	0.989	0.989 ± 0.007
MobileNetV3Small	0.977	0.989	0.977	0.977	0.983	0.981 ± 0.005
MobileNetV3Large	0.983	0.983	1.000	0.989	0.983	0.988 ± 0.007

TABLE 3. Training/validation performance (MEAN ± SD) for five-fold cross-validation.

Transferred Pre-trained Models	Training Accuracy	Training Loss	Validation Accuracy	Validation Loss
ResNet50	0.998 ± 0.001	0.015 ± 0.006	0.989 ± 0.007	0.035 ± 0.016
MobileNetV3Small	0.997 ± 0.002	0.018 ± 0.005	0.981 ± 0.005	0.043 ± 0.007
MobileNetV3Large	0.997 ± 0.003	0.016 ± 0.006	0.988 ± 0.007	0.033 ± 0.015

TABLE 4. Performance metrics (MEAN ± SD) for five-fold cross-validation on the validation dataset.

Transferred Pre-trained Models	Accuracy	Recall	Specificity	Precision	F1 Score	AUC
ResNet50	0.989 ± 0.007	0.986 ± 0.010	0.990 ± 0.012	0.992 ± 0.008	0.989 ± 0.007	0.988 ± 0.008
MobileNetV3Small	0.981 ± 0.005	0.978 ± 0.007	0.984 ± 0.007	0.984 ± 0.006	0.981 ± 0.004	0.981 ± 0.005
MobileNetV3Large	0.988 ± 0.007	0.986 ± 0.016	0.988 ± 0.012	0.989 ± 0.011	0.987 ± 0.008	0.987 ± 0.008

TABLE 5. Performance metrics (MEAN ± SD) for five-fold cross-validation on the test dataset.

Transferred Pre-trained Models	Accuracy	Recall	Specificity	Precision	F1 Score	AUC
ResNet50	0.982 ± 0.015	0.995 ± 0.012	0.971 ± 0.027	0.969 ± 0.027	0.981 ± 0.015	0.983 ± 0.014
MobileNetV3Small	0.982 ± 0.011	0.973 ± 0.027	0.990 ± 0.013	0.989 ± 0.015	0.981 ± 0.012	0.982 ± 0.012
MobileNetV3Large	0.992 ± 0.007	1.000 ± 0.000	0.985 ± 0.013	0.984 ± 0.014	0.992 ± 0.007	0.993 ± 0.007

Figure 6 shows the Accuracy and Loss plots of the Training and Validation for five folds of the transferred CNN based on MobileNetV3Small. Table 2 presents the classification accuracies of the transferred CNN models on the validation dataset for each of the five folds, along with the classification accuracy averaged over the five folds. Table 3 highlights the

performance of the models during training and validation, averaging over five folds. Table 4 summarizes the detailed classification performance of the models on the validation dataset, averaging over five folds. Figure 7 reports the confusion matrices, and Table 5 reports the overall model’s performance on the test (unseen) data, averaging over the five folds.

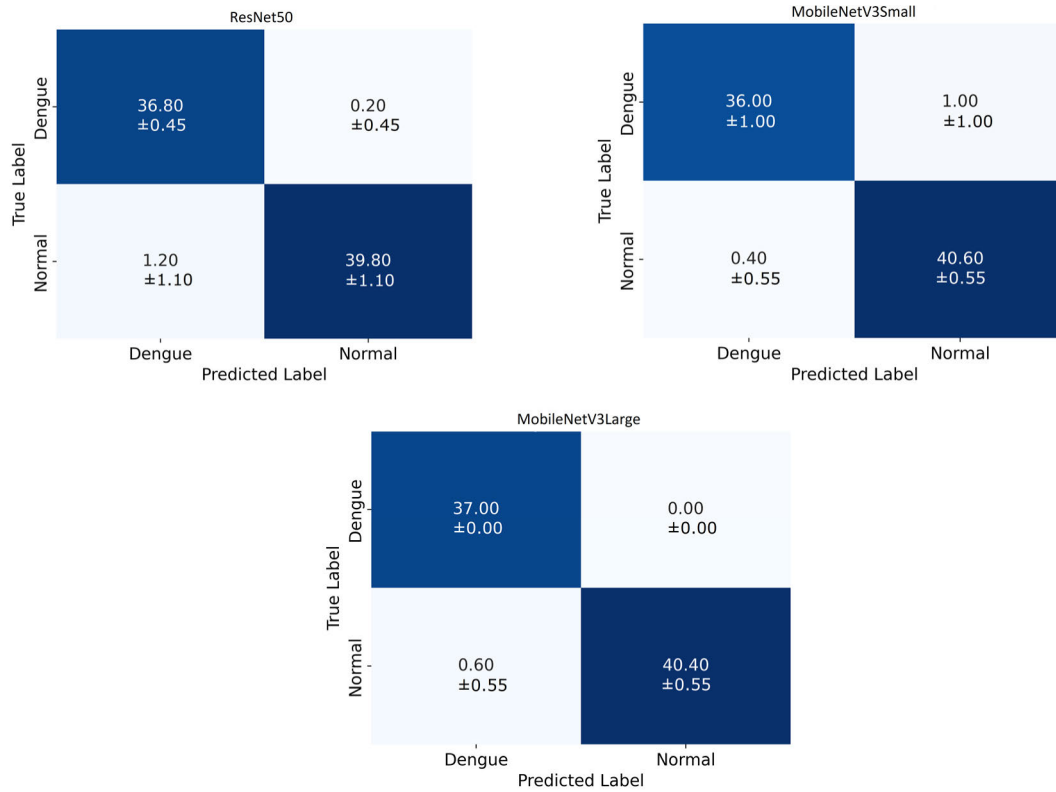


FIGURE 7. Confusion matrices (Mean ± SD) for five-fold cross-validation on the test dataset of the transferred pre-trained CNN based on (a) ResNet50, (b) MobileNetV3Small, and (c) MobileNetV3Large.

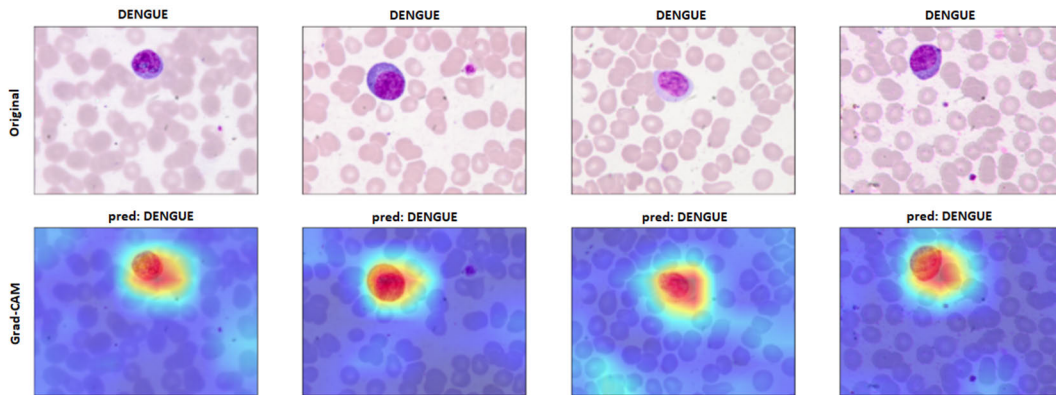


FIGURE 8. Activation map for Dengue class obtained from the GradCAM technique for the transferred pre-trained CNN based on ResNet50.

While all models rendered good performance (above 98% overall classification accuracy), MobileNetV3Small is the recommended model for this classification problem due to its significantly less computationally demanding characteristics. MobileNetV3Small is characterized by limited parameters, i.e., approx. 2.9 million, and therefore is the least time-consuming and has the least resource requirement.

Figures 8 and 9 demonstrate the GradCAM localization of the areas of the image that are most valuable for the predictions. As a result, the proposed transferred pre-trained CNN models (for example, based on ResNet50) recognized the changes in the morphology of the lymphocytes in Figure 8 and highlighted it with an activation map, demonstrating that

it is the noteworthy region of interest for the identification of Dengue class in the image. Instead, as indicated in Figure 9, the model for the Normal class did not highlight the lymphocyte region, indicating no morphological changes in the lymphocyte. The red/yellow color in the activation maps indicated more concentrated regions, and the less concentrated regions are with lighter colors approaching green/blue.

The outcomes of this work are inspiring and demonstrate that the pre-trained CNNs have the capacity to yield commendable assistance in the PBS analysis for dengue diagnosis. This work is crucial and can contribute significantly to healthcare as this offers some level of explainability of the inner workings of the CNNs that clinicians may

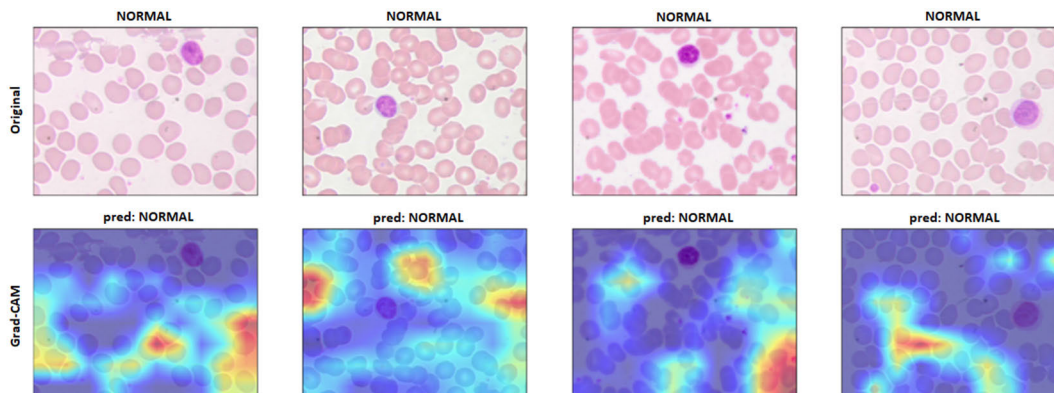


FIGURE 9. Activation map for Normal class obtained from the GradCAM technique for the transferred pre-trained CNN based on ResNet50.

TABLE 6. Comparison of the proposed work with the state-of-the-art works from the literature.

Author (Ref.)	Input /data	Model	Cross-Validation	XAI technique	Accuracy
Gambhir et al. (2017)[55]	symptoms, vital signs, and blood profile data (tabular data)	ML - PSO optimized ANN	Yes	No	87.27%
Mello-Roman et al. (2019)[35]	symptoms (tabular data)	ML - MLP	No	No	96.00%
Katta et al. (2021)[33]	symptoms (tabular data)	ML - RF	No	No	94.39%
Mayrose et al. (2021)[37]	Deep/LBP features from PBS images	ML - SVM	Yes	No	95.74%
Hoyos et al. (2022)[36]	symptoms, vital signs, and blood profile data (tabular data)	ML - FCM	Yes	No	89.40%
Mayrose et al. (2023)[38]	morphological/GLCM features from PBS images	ML - SVM	Yes	No	93.62%
Proposed work	PBS images	DL - transferred pre-trained CNNs	Yes	Yes	> 98.00%

relate to. Moreover, this work is better in the context that it bypasses laborious steps like segmentation of lymphocyte nucleus, feature extraction, and feature ranking, in contrast to the classical machine learning methods. In one of our previous works [38], ten, morphological and GLCM features were extracted from the segmented lymphocyte nucleus. These features, when coupled with SVM, achieved the best classification with Accuracy, Recall, Specificity, Precision, F1 Score, and AUC of 93.62%, 92.59%, 95%, 96.15%, 94.34%, and 0.96, respectively. Furthermore, this work differs from works in that the authors have taken advantage of pre-trained CNNs as feature extractors and linked them

to a separate machine-learning classifier. In another previous work [37], 1,000 deep and 177 Local Binary Pattern generated features were derived from the segmented lymphocyte nucleus. Deep features were derived by utilizing pre-trained CNN MobileNetV2 as a feature extractor. Feature selection algorithm ReliefF was used to select 100 important features. These features given to SVM yielded the best classification with accuracy, recall, specificity, precision, F1 Score, and AUC of 95.74%, 98.15%, 92.50%, 94.64%, 96.36%, and 0.98, respectively. The model’s performance can be further boosted by exploring different fine-tuning strategies.

There was a dearth of existing publications employing PBS images for dengue diagnosis, and the literature review revealed no published works from other research groups utilizing similar methodologies on comparable datasets. Most of the research work reported on automated diagnosis of dengue is by utilizing symptoms, vital signs, blood profile data, or a combination of these. Gambhir et al. proposed a PSO-optimized ANN for the diagnosis of dengue. With 16 attributes containing symptoms, vital signs, and blood profile data, authors classified the data and documented an accuracy, recall, and specificity of 87.27%, 68%, and 92.94%, respectively [55]. Mello-Roman et al. developed a symptom-based diagnostic model for dengue fever. With 38 attributes, including symptoms, the authors classified the data using MLP and documented an accuracy, recall, and specificity of 96%, 96%, and 97%, respectively [35]. Katta et al. used symptoms to develop an efficient model for dengue detection. The RF classifier yielded an accuracy and sensitivity of 94.39% and 95.60%, respectively [33]. Hoyos et al. developed a decision-support system for dengue diagnosis using the fuzzy cognitive map. With 22 features, including symptoms, vital signs, and blood profile data, the authors achieved a classification accuracy of 89.40% [36]. Table 6 summarizes the comparison of the performance of the proposed work with other works on automated detection of dengue published in the literature.

This work incorporates an end-to-end computationally efficient DL system for automatically detecting dengue from PBS. The system is integrated with GradCAM explainability and utilizes data sourced authentically from Kasturba Hospital, Manipal, under ethical clearance. Certainly, the entries in Table 6 depict that the proposed method for dengue diagnosis outperformed in comparison with the state-of-the-art studies published in the literature.

IV. CONCLUSION AND FUTURE WORK

The examination of the PBS is a powerful adjunct to other clinical procedures. In connection with dengue diagnosis, it can be a crucial add-on to the Complete Blood Count test and NS1 antigen capture and can substantially aid dengue diagnosis in low-resource settings. This work utilizes pre-trained CNNs for dengue fever detection from digital microscopic PBS images. The transfer learning strategy was successful in differentiating dengue-infected and normal smears. All three models rendered good performance with classification accuracy above 98%. Despite being less computationally expensive, the performance of the transferred pre-trained CNN based on MobileNetV3Small is at par with the other two models. Hence, transferred pre-trained CNN based on MobileNetV3Small is the preferred model for the proposed method of dengue diagnosis. Explainability is recognized as a key component for the acceptance of AI systems for clinical use. An explainability technique - GradCAM was integrated to the models to visualize the specific regions of the smears that were most dominant in making the predictive decisions. Promising

results show that the developed models have the potential to provide high-quality support to haematologists by expertly executing tedious, repetitive, and time-consuming duties in hospitals and remote/low-resource settings. Future works could be focused on examining different fine-tuning strategies to facilitate performance improvement. The dataset size (multiple hospital data) could be further improved to increase the algorithm's robustness. Moreover, a multiclass problem could be considered for analyzing dengue severity (normal/mild dengue/severe dengue). Furthermore, in the future, our method could be incorporated into mobile devices with a microscope attachment and utilized as a standalone product to screen for dengue in hospitals.

ACKNOWLEDGMENT

The authors thank the Department of Pathology, Kasturba Hospital, MAHE, Manipal, for providing the peripheral blood smear slides and a digital microscope to capture the peripheral blood smear images required for this work. They also would like to thank the Department of Immunohaematology, Kasturba Hospital, MAHE, Manipal, for providing blood samples from healthy blood bank donors.

REFERENCES

- [1] CDC. *About Dengue*. Accessed: Aug. 15, 2023. [Online]. Available: <https://www.cdc.gov/dengue/about/index.html>
- [2] N. Mondal, "The resurgence of dengue epidemic and climate change in India," *Lancet*, vol. 401, no. 10378, pp. 727–728, Mar. 2023, doi: [10.1016/s0140-6736\(23\)00226-x](https://doi.org/10.1016/s0140-6736(23)00226-x).
- [3] WHO. *Dengue and Severe Dengue*. Accessed: Aug. 15, 2023. [Online]. Available: <https://www.who.int/news-room/fact-sheets/detail/dengue-and-severe-dengue>
- [4] S. J. Thomas, "Is new dengue vaccine efficacy data a relief or cause for concern?" *NPJ Vaccines*, vol. 8, no. 1, p. 55, Apr. 2023, doi: [10.1038/s41541-023-00658-2](https://doi.org/10.1038/s41541-023-00658-2).
- [5] D. A. Müller, A. C. I. Depelsenaire, and P. R. Young, "Clinical and laboratory diagnosis of dengue virus infection," *J. Infectious Diseases*, vol. 215, no. 2, pp. S89–S95, Mar. 2017, doi: [10.1093/infdis/jiw649](https://doi.org/10.1093/infdis/jiw649).
- [6] H. A. Alhazmi, W. Ahsan, M. M. E. Taha, M. Albratty, A. Najmi, A. Farasani, A. A. Abdulhaq, and I. A. Darwish, "Development of screen-printed carbon electrode-based immunosensors for the electrochemical detection of dengue virus antigen," *J. King Saud Univ.-Sci.*, vol. 35, no. 3, Apr. 2023, Art. no. 102568, doi: [10.1016/j.jksus.2023.102568](https://doi.org/10.1016/j.jksus.2023.102568).
- [7] A. Garg, J. Garg, D. Singh, and T. Dhole, "Can rapid dengue diagnostic kits be trusted? A comparative study of commercially available rapid kits for serodiagnosis of dengue fever," *J. Lab. Physicians*, vol. 11, no. 1, pp. 63–67, Jan. 2019, doi: [10.4103/jlp.jlp_140_18](https://doi.org/10.4103/jlp.jlp_140_18).
- [8] K. Prasad and B. M. K. Singh, "Analysis of red blood cells from peripheral blood smear images for anemia detection: A methodological review," *Med. Biol. Eng. Comput.*, vol. 60, no. 9, pp. 2445–2462, Sep. 2022, doi: [10.1007/s11517-022-02614-z](https://doi.org/10.1007/s11517-022-02614-z).
- [9] F. I. F. Escobar, J. R. T. Alipo-On, J. L. U. Novia, M. J. T. Tan, H. A. Karim, and N. AlDahoul, "Automated counting of white blood cells in thin blood smear images," *Comput. Electr. Eng.*, vol. 108, May 2023, Art. no. 108710, doi: [10.1016/j.compeleceng.2023.108710](https://doi.org/10.1016/j.compeleceng.2023.108710).
- [10] M. Salvi, U. R. Acharya, F. Molinari, and K. M. Meiburger, "The impact of pre- and post-image processing techniques on deep learning frameworks: A comprehensive review for digital pathology image analysis," *Comput. Biol. Med.*, vol. 128, Jan. 2021, Art. no. 104129, doi: [10.1016/j.compbiomed.2020.104129](https://doi.org/10.1016/j.compbiomed.2020.104129).
- [11] W. Walter, C. Pohlkamp, M. Megendorfer, N. Nadarajah, W. Kern, C. Haferlach, and T. Haferlach, "Artificial intelligence in hematological diagnostics: Game changer or gadget?" *Blood Rev.*, vol. 58, Mar. 2023, Art. no. 101019, doi: [10.1016/j.blre.2022.101019](https://doi.org/10.1016/j.blre.2022.101019).

- [12] P. Kora, C. P. Ooi, O. Faust, U. Raghavendra, A. Gudigar, W. Y. Chan, K. Meenakshi, K. Swaraja, P. Plawiak, and U. Rajendra Acharya, "Transfer learning techniques for medical image analysis: A review," *Biocybernetics Biomed. Eng.*, vol. 42, no. 1, pp. 79–107, Jan. 2022, doi: [10.1016/j.bbe.2021.11.004](https://doi.org/10.1016/j.bbe.2021.11.004).
- [13] I. Collieran, J. Vignarajan, S. Frost, and S. Saha, "Evaluating the performance of different convolutional neural networks in glaucoma detection," in *Proc. Int. Conf. Digit. Image Comput., Techn. Appl. (DICTA)*, Nov. 2022, pp. 1–5, doi: [10.1109/DICTA56598.2022.10034616](https://doi.org/10.1109/DICTA56598.2022.10034616).
- [14] L. Alzubaidi, J. Zhang, A. J. Humaidi, A. Al-Dujaili, Y. Duan, O. Al-Shamma, J. Santamaría, M. A. Fadhel, M. Al-Amidie, and L. Farhan, "Review of deep learning: Concepts, CNN architectures, challenges, applications, future directions," *J. Big Data*, vol. 8, no. 1, p. 53, Mar. 2021, doi: [10.1186/s40537-021-00444-8](https://doi.org/10.1186/s40537-021-00444-8).
- [15] R. R. Selvaraju, M. Cogswell, A. Das, R. Vedantam, D. Parikh, and D. Batra, "Grad-CAM: Visual explanations from deep networks via gradient-based localization," in *Proc. IEEE Int. Conf. Comput. Vis. (ICCV)*, Oct. 2017, pp. 618–626, doi: [10.1109/ICCV.2017.74](https://doi.org/10.1109/ICCV.2017.74).
- [16] V. Jahmunah, E. Y. K. Ng, R.-S. Tan, S. L. Oh, and U. R. Acharya, "Explainable detection of myocardial infarction using deep learning models with grad-CAM technique on ECG signals," *Comput. Biol. Med.*, vol. 146, Jul. 2022, Art. no. 105550, doi: [10.1016/j.compbiomed.2022.105550](https://doi.org/10.1016/j.compbiomed.2022.105550).
- [17] H. W. Loh, C. P. Ooi, S. Seoni, P. D. Barua, F. Molinari, and U. R. Acharya, "Application of explainable artificial intelligence for healthcare: A systematic review of the last decade (2011–2022)," *Comput. Methods Programs Biomed.*, vol. 226, Nov. 2022, Art. no. 107161, doi: [10.1016/j.cmpb.2022.107161](https://doi.org/10.1016/j.cmpb.2022.107161).
- [18] J. A. Marmolejo-Saucedo and U. Kose, "Numerical grad-cam based explainable convolutional neural network for brain tumor diagnosis," *Mobile Netw. Appl.*, vol. 2022, pp. 1–10, Aug. 2022, doi: [10.1007/s11036-022-02021-6](https://doi.org/10.1007/s11036-022-02021-6).
- [19] B. Zhou, A. Khosla, A. Lapedriza, A. Oliva, and A. Torralba, "Learning deep features for discriminative localization," in *Proc. IEEE Conf. Comput. Vis. Pattern Recognit. (CVPR)*, Jun. 2016, pp. 2921–2929, doi: [10.1109/CVPR.2016.319](https://doi.org/10.1109/CVPR.2016.319).
- [20] A. Saranya and R. Subhashini, "A systematic review of explainable artificial intelligence models and applications: Recent developments and future trends," *Decis. Anal. J.*, vol. 7, Jun. 2023, Art. no. 100230, doi: [10.1016/j.dajour.2023.100230](https://doi.org/10.1016/j.dajour.2023.100230).
- [21] S. Aziz, M. Bilal, M. U. Khan, and F. Amjad, "Deep learning-based automatic morphological classification of leukocytes using blood smears," in *Proc. Int. Conf. Electr., Commun., Comput. Eng. (ICECCE)*, Jun. 2020, pp. 1–5, doi: [10.1109/ICECCE49384.2020.9179246](https://doi.org/10.1109/ICECCE49384.2020.9179246).
- [22] M. R. Reena and P. M. Ameer, "Localization and recognition of leukocytes in peripheral blood: A deep learning approach," *Comput. Biol. Med.*, vol. 126, Nov. 2020, Art. no. 104034, doi: [10.1016/j.compbiomed.2020.104034](https://doi.org/10.1016/j.compbiomed.2020.104034).
- [23] K. Almezghwi and S. Serte, "Improved classification of white blood cells with the generative adversarial network and deep convolutional neural network," *Comput. Intell. Neurosci.*, vol. 2020, pp. 1–12, Jul. 2020, doi: [10.1155/2020/6490479](https://doi.org/10.1155/2020/6490479).
- [24] L. Ma, R. Shuai, X. Ran, W. Liu, and C. Ye, "Combining DC-GAN with ResNet for blood cell image classification," *Med. Biol. Eng. Comput.*, vol. 58, no. 6, pp. 1251–1264, Jun. 2020, doi: [10.1007/s11517-020-02163-3](https://doi.org/10.1007/s11517-020-02163-3).
- [25] S. Sharma, S. Gupta, D. Gupta, S. Juneja, P. Gupta, G. Dhiman, and S. Kautish, "Deep learning model for the automatic classification of white blood cells," *Comput. Intell. Neurosci.*, vol. 2022, pp. 1–13, Jan. 2022, doi: [10.1155/2022/7384131](https://doi.org/10.1155/2022/7384131).
- [26] E. Cengil, A. Çınar, and M. Yıldırım, "A hybrid approach for efficient multi-classification of white blood cells based on transfer learning techniques and traditional machine learning methods," *Concurrency Comput., Pract. Exper.*, vol. 34, no. 6, p. e6756, Mar. 2022, doi: [10.1002/cpe.6756](https://doi.org/10.1002/cpe.6756).
- [27] R. Liu, W. Dai, T. Wu, M. Wang, S. Wan, and J. Liu, "AIMIC: Deep learning for microscopic image classification," *Comput. Methods Programs Biomed.*, vol. 226, Nov. 2022, Art. no. 107162, doi: [10.1016/j.cmpb.2022.107162](https://doi.org/10.1016/j.cmpb.2022.107162).
- [28] H. Chen, J. Liu, C. Hua, J. Feng, B. Pang, D. Cao, and C. Li, "Accurate classification of white blood cells by coupling pre-trained ResNet and DenseNet with SCAM mechanism," *BMC Bioinf.*, vol. 23, no. 1, p. 282, Dec. 2022, doi: [10.1186/s12859-022-04824-6](https://doi.org/10.1186/s12859-022-04824-6).
- [29] A. Meenakshi, J. A. Ruth, V. R. Kanagavalli, and R. Uma, "Automatic classification of white blood cells using deep features based convolutional neural network," *Multimedia Tools Appl.*, vol. 81, no. 21, pp. 30121–30142, Sep. 2022, doi: [10.1007/s11042-022-12539-2](https://doi.org/10.1007/s11042-022-12539-2).
- [30] N. Dong, Q. Feng, J. Chang, and X. Mai, "White blood cell classification based on a novel ensemble convolutional neural network framework," *J. Supercomput.*, vol. 80, no. 1, pp. 249–270, Jun. 2023, doi: [10.1007/s11227-023-05490-y](https://doi.org/10.1007/s11227-023-05490-y).
- [31] S. M. Dipto, M. T. Reza, M. N. J. Rahman, M. Z. Parvez, P. D. Barua, and S. Chakraborty, "An XAI integrated identification system of white blood cell type using variants of vision transformer," in *Proc. 2nd Int. Conf. Innov. Comput. Res.*, 2023, pp. 303–315, doi: [10.1007/978-3-031-35308-6_26](https://doi.org/10.1007/978-3-031-35308-6_26).
- [32] K. Bhatia, S. Dhalla, A. Mittal, S. Gupta, A. Gupta, and A. Jindal, "Integrating explainability into deep learning-based models for white blood cells classification," *Comput. Electr. Eng.*, vol. 110, Sep. 2023, Art. no. 108913, doi: [10.1016/j.compeleceng.2023.108913](https://doi.org/10.1016/j.compeleceng.2023.108913).
- [33] M. Katta, R. Sandanalakshmi, G. Srilakshmi, and R. Adireddi, "An efficient learning model selection for dengue detection," in *Intelligent and Cloud Computing (Smart Innovation, Systems and Technologies)*. Singapore: Springer, 2022, pp. 439–453, doi: [10.1007/978-981-16-9873-6_40](https://doi.org/10.1007/978-981-16-9873-6_40).
- [34] A. Sajid and M. A. Awan, "Monitoring, tracking and diagnosing dengue fever using smartphone, GPS and machine learning," in *Proc. 16th Int. Conf. Emerg. Technol. (ICET)*, Dec. 2021, pp. 1–6, doi: [10.1109/ICET54505.2021.9689785](https://doi.org/10.1109/ICET54505.2021.9689785).
- [35] J. D. Mello-Román, J. C. Mello-Román, S. Gómez-Guerrero, and M. García-Torres, "Predictive models for the medical diagnosis of dengue: A case study in Paraguay," *Comput. Math. Methods Med.*, vol. 2019, pp. 1–7, Jul. 2019, doi: [10.1155/2019/7307803](https://doi.org/10.1155/2019/7307803).
- [36] W. Hoyos, J. Aguilar, and M. Toro, "A clinical decision-support system for dengue based on fuzzy cognitive maps," *Health Care Manage. Sci.*, vol. 25, no. 4, pp. 666–681, Aug. 2022, doi: [10.1007/s10729-022-09611-6](https://doi.org/10.1007/s10729-022-09611-6).
- [37] H. Mayrose, N. Sampathila, G. M. Bairy, S. Belurkar, K. Saravu, A. Basu, and S. Khan, "Intelligent algorithm for detection of dengue using MobileNetV2-based deep features with lymphocyte nucleus," *Expert Syst.*, vol. 40, no. 4, Nov. 2021, Art. no. e12904, doi: [10.1111/exsy.12904](https://doi.org/10.1111/exsy.12904).
- [38] H. Mayrose, G. M. Bairy, N. Sampathila, S. Belurkar, and K. Saravu, "Machine learning-based detection of dengue from blood smear images utilizing platelet and lymphocyte characteristics," *Diagnostics*, vol. 13, no. 2, p. 220, Jan. 2023, doi: [10.3390/diagnostics13020220](https://doi.org/10.3390/diagnostics13020220).
- [39] Y. Tanaka, "Plasmacytoid lymphocytes: A diagnostic clue for dengue fever," *Internal Med.*, vol. 57, no. 19, p. 2917, Oct. 2018, doi: [10.2169/internalmedicine.0179-17](https://doi.org/10.2169/internalmedicine.0179-17).
- [40] S. Pathan, P. C. Siddalingaswamy, P. Kumar, M. Pai M M, T. Ali, and U. R. Acharya, "Novel ensemble of optimized CNN and dynamic selection techniques for accurate COVID-19 screening using chest CT images," *Comput. Biol. Med.*, vol. 137, Oct. 2021, Art. no. 104835, doi: [10.1016/j.compbiomed.2021.104835](https://doi.org/10.1016/j.compbiomed.2021.104835).
- [41] K. He, X. Zhang, S. Ren, and J. Sun, "Deep residual learning for image recognition," in *Proc. IEEE Conf. Comput. Vis. Pattern Recognit. (CVPR)*, Jun. 2016, pp. 770–778, doi: [10.1109/CVPR.2016.90](https://doi.org/10.1109/CVPR.2016.90).
- [42] A. A. Ardakani, A. R. Kanafi, U. R. Acharya, N. Khadem, and A. Mohammadi, "Application of deep learning technique to manage COVID-19 in routine clinical practice using CT images: Results of 10 convolutional neural networks," *Comput. Biol. Med.*, vol. 121, Jun. 2020, Art. no. 103795, doi: [10.1016/j.compbiomed.2020.103795](https://doi.org/10.1016/j.compbiomed.2020.103795).
- [43] S. Dogan, P. Datta Barua, H. Kutlu, M. Baygin, H. Fujita, T. Tuncer, and U. R. Acharya, "Automated accurate fire detection system using ensemble pretrained residual network," *Expert Syst. Appl.*, vol. 203, Oct. 2022, Art. no. 117407, doi: [10.1016/j.eswa.2022.117407](https://doi.org/10.1016/j.eswa.2022.117407).
- [44] M. Talo, O. Yildirim, U. B. Baloglu, G. Aydin, and U. R. Acharya, "Convolutional neural networks for multi-class brain disease detection using MRI images," *Computerized Med. Imag. Graph.*, vol. 78, Dec. 2019, Art. no. 101673, doi: [10.1016/j.compmedimag.2019.101673](https://doi.org/10.1016/j.compmedimag.2019.101673).
- [45] X. Bao, Y. Xu, H.-K. Lam, M. Trabelsi, I. Chihai, L. Sidhom, and E. N. Kamavuako, "Time-frequency distributions of heart sound signals: A comparative study using convolutional neural networks," *Biomed. Eng. Adv.*, vol. 5, Jun. 2023, Art. no. 100093, doi: [10.1016/j.bea.2023.100093](https://doi.org/10.1016/j.bea.2023.100093).
- [46] A. A. Smadi, A. Abugabah, A. M. Al-smadi, and S. Almotairi, "SEL-COVIDNET: An intelligent application for the diagnosis of COVID-19 from chest X-rays and CT-scans," *Informat. Med. Unlocked*, vol. 32, Jun. 2022, Art. no. 101059, doi: [10.1016/j.imu.2022.101059](https://doi.org/10.1016/j.imu.2022.101059).

- [47] A. Howard, M. Sandler, B. Chen, W. Wang, L.-C. Chen, M. Tan, G. Chu, V. Vasudevan, Y. Zhu, R. Pang, H. Adam, and Q. Le, "Searching for MobileNetV3," in *Proc. IEEE/CVF Int. Conf. Comput. Vis. (ICCV)*, Oct. 2019, pp. 1314–1324, doi: [10.1109/ICCV.2019.00140](https://doi.org/10.1109/ICCV.2019.00140).
- [48] G. Pazzaglia, M. Mameli, L. Rossi, M. Paolanti, A. Mancini, P. Zingaretti, and E. Frontoni, "People counting on low cost embedded hardware during the SARS-CoV-2 pandemic," in *Proc. ICPR Int. Workshops Challenges*, 2021, pp. 521–533, doi: [10.1007/978-3-030-68790-8_41](https://doi.org/10.1007/978-3-030-68790-8_41).
- [49] S. Qian, C. Ning, and Y. Hu, "MobileNetV3 for image classification," in *Proc. IEEE 2nd Int. Conf. Big Data, Artif. Intell. Internet Things Eng. (ICBAIE)*, Mar. 2021, pp. 490–497, doi: [10.1109/ICBAIE52039.2021.9389905](https://doi.org/10.1109/ICBAIE52039.2021.9389905).
- [50] A. Cardellicchio, S. Ruggieri, A. Nettis, V. Renò, and G. Uva, "Physical interpretation of machine learning-based recognition of defects for the risk management of existing bridge heritage," *Eng. Failure Anal.*, vol. 149, Jul. 2023, Art. no. 107237, doi: [10.1016/j.engfailanal.2023.107237](https://doi.org/10.1016/j.engfailanal.2023.107237).
- [51] R. Yamashita, M. Nishio, R. K. G. Do, and K. Togashi, "Convolutional neural networks: An overview and application in radiology," *Insights Imag.*, vol. 9, no. 4, pp. 611–629, Aug. 2018, doi: [10.1007/s13244-018-0639-9](https://doi.org/10.1007/s13244-018-0639-9).
- [52] M. Masud, A. E. Eldin Rashed, and M. S. Hossain, "Convolutional neural network-based models for diagnosis of breast cancer," *Neural Comput. Appl.*, vol. 34, no. 14, pp. 11383–11394, Jul. 2022, doi: [10.1007/s00521-020-05394-5](https://doi.org/10.1007/s00521-020-05394-5).
- [53] J.-K. Kim, S. Jung, J. Park, and S. W. Han, "Arrhythmia detection model using modified DenseNet for comprehensible grad-CAM visualization," *Biomed. Signal Process. Control*, vol. 73, Mar. 2022, Art. no. 103408, doi: [10.1016/j.bspc.2021.103408](https://doi.org/10.1016/j.bspc.2021.103408).
- [54] A. Abhishek, R. K. Jha, R. Sinha, and K. Jha, "Automated detection and classification of leukemia on a subject-independent test dataset using deep transfer learning supported by grad-CAM visualization," *Biomed. Signal Process. Control*, vol. 83, May 2023, Art. no. 104722, doi: [10.1016/j.bspc.2023.104722](https://doi.org/10.1016/j.bspc.2023.104722).
- [55] S. Gambhir, S. K. Malik, and Y. Kumar, "PSO-ANN based diagnostic model for the early detection of dengue disease," *New Horizons Transl. Med.*, vol. 4, no. 1, pp. 1–8, Nov. 2017, doi: [10.1016/j.nhtm.2017.10.001](https://doi.org/10.1016/j.nhtm.2017.10.001).



HILDA MAYROSE received the B.E. and M.Tech. degrees in biomedical engineering from Manipal Institute of Technology (MIT), Manipal, in 1997 and 1999, respectively, where she is currently pursuing the Ph.D. degree (part-time) with the Department of Biomedical Engineering. She is currently an Assistant Professor (Senior Scale) with the Department of Biomedical Engineering, Manipal Academy of Higher Education (MAHE), MIT. She has more than 20 years of experience

in teaching with the Department of Biomedical Engineering. Her research interests include biomedical instrumentation, biomedical signal and image analysis, and machine and deep learning applications in healthcare.



NIRANJANA SAMPATHILA (Senior Member, IEEE) received the B.E. degree in electronics and engineering and the M.Tech. degree in biomedical engineering from Mangalore University and the Ph.D. degree from Manipal University [currently known as the Manipal Academy of Higher Education (MAHE)], Manipal, India. He has more than 25 years of experience in research and academics in biomedical engineering applications. He is currently an Additional Professor with Manipal

Institute of Technology, MAHE. He has published a good number of papers in journals and conferences. His research interests include pattern recognition, medical informatics, miniaturized system design, nanoelectronics, and AI for healthcare. He is a fellow of IE, India.



G. MURALIDHAR BAIRY (Senior Member, IEEE) received the B.E. degree in electronics and communication engineering and the M.Tech. degree in biomedical engineering from Mangalore University and the Ph.D. degree from Manipal Academy of Higher Education, Manipal, India. He has more than 33 years of experience in research and academics in biomedical engineering applications. He is currently the HOD and an Additional Professor with the Biomedical Engineering Department, Manipal Institute of Technology, Manipal Academy of Higher Education. He has published a good number of papers in Scopus-indexed journals and conferences. His research interests include biomedical signal and image processing, biomedical instrumentation, and AI for healthcare.

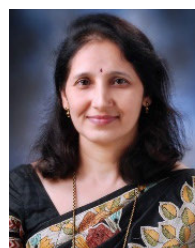


TUSHAR NAYAK (Member, IEEE) received the B.Tech. degree in biomedical engineering from Manipal Institute of Technology (MIT), Manipal Academy of Higher Education (MAHE), Manipal, in 2023. He is currently a Research Associate with IIT Hyderabad. His research interests include signal and image processing, machine learning, and deep learning applications in healthcare.



SUSHMA BELURKAR received the M.D. Pathology degree from Goa University. She is currently an Additional Professor of pathology with the Kasturba Medical College, MAHE, Manipal, India, and also in charge of the Hematology and Clinical Pathology Laboratory. She has more than 20 years of experience in teaching, diagnostics, and research. In the last 20 years, she has guided 12 students in the M.D. thesis and mentored five student projects and is a co-guide for four Ph.D.

students. She has been the co-investigator in four funded projects. She has more than 50 publications in national and international journals. Her research interests include anemia, leukemia, bleeding disorders, and quality control.



KAVITHA SARAVU is currently a Professor and the Head of the Department of Infectious Diseases, Kasturba Medical College, Manipal, and the Coordinator of Manipal Center for Infectious Diseases (MACID). She has additional training in tropical medicine with LSHTM, London, and training in translational research in infectious diseases with the Yale School of Medicine, USA. She has clinical and research expertise in infectious diseases, particularly tropical infections, like malaria, scrub typhus, Kyasanur forest disease (KFD), melioidosis, COVID-19, TB, and HIV. For the last 23 years, she has supervised more than 75 student projects, mentored 25 students in the M.D. thesis, and guided the seven Ph.D. students. She has mentored six overseas students from Canada and Germany. She has around 150 peer-reviewed publications, including in *The Lancet Infectious Diseases* and *The New England Journal of Medicine*. Her research interests include severity, antimalarial resistance, relapses in malaria, immune response, and treatment of severe scrub typhus, TB-DM, diagnosis of EPTB, computer-aided radiography for PTB, malnutrition and TB, and disease characterization of monkey fever "Kyasanur forest disease."

...